SCIENTIFIC REPORTS

OPEN

Quantitative determination and toxicity evaluation of 2,4-dichlorophenol using poly(eosin Y)/hydroxylated multi-walled carbon nanotubes modified electrode

Xiaolin Zhu[1], Kexin Zhang[1], Chengzhi Wang[1], Jiunian Guan[1], Xing Yuan[1,*] & Baikun Li[2,*]

This study aimed at developing simple, sensitive and rapid electrochemical approach to quantitatively determine and assess the toxicity of 2,4-dichlorophenol (2,4-DCP), a priority pollutant and has potential risk to public health through a novel poly(eosin Y, EY)/hydroxylated multi-walled carbon nanotubes composite modified electrode (PEY/MWNTs-OH/GCE). The distinct feature of this easy-fabricated electrode was the synergistic coupling effect between EY and MWNTs-OH that enabled a high electrocatalytic activity to 2,4-DCP. Under optimum conditions, the oxidation peak current enhanced linearly with concentration increasing from 0.005 to 0.1 μM and 0.2 to 40.0 μM, and revealed the detection limit of 1.5 nM. Moreover, the PEY/MWNTs-OH/GCE exhibited excellent electrocatalytic activity toward intracellular electroactive species. Two sensitive electrochemical signals ascribed to guanine/xanthine and adenine/hypoxanthine in human hepatoma (HepG2) cells were detected simultaneously. The sensor was successfully applied to evaluate the toxicity of 2,4-DCP to HepG2 cells. The IC_{50} values based on the two electrochemical signals are 201.07 and 252.83 μM, respectively. This study established a sensitive platform for the comprehensive evaluation of 2,4-DCP and posed a great potential to simplify environmental toxicity monitoring.

2,4-dichlorophenol (2,4-DCP) is a typical chlorophenol compound widely used in herbicides, fungicides, and insecticides[1]. As a priority pollutant listed by the US Environment Protection Agency (EPA), 2,4-DCP seriously threatens environmental quality and public health[2,3]. Despite the maximum permissible concentration of 2,4-DCP in drinking water is set as 0.5 mg L^{-1}, higher concentrations are usually found in polluted environments[4,5]. Until now, there has been no quantitative determination and toxicity evaluation method for early detection of 2,4-DCP. Due to its low allowable concentration and coexistence with interfering substances (e.g. phenols and metal ions), 2,4-DCP has been measured using UV spectrophotometry[6], gas chromatography[7], high-performance liquid chromatography[8], and capillary electrophoresis[9]. However, most of these methods are complex, low sensitive, costly, and incapable of real-time monitoring. The electrochemical method newly developed is preferable owing to the simplicity, high sensitivity, low-cost, and continuous on-line detection[10–15].

As for the *in vitro* toxicity evaluation of pollutants, some techniques such as the 3-(4,5-dimethylthiazol-2-yl)-2, 5-diphenyltetrazolium bromide (MTT) assay[16], flow cytometry experiment[17], and lactate dehydrogenase (LDH) release assay[18] have been developed. Recently, cell-based electrochemical method that is simple, sensitive, rapid, label-free, and non-toxic has gained attention for toxicity assessment[19–21]. An *in-situ* electrochemical method was successfully developed and applied in drug screening and toxicity evaluation of heavy metals in our previous

[1]School of Environment, Northeast Normal University, Changchun 130117, P.R. China. [2]Department of Civil and Environmental Engineering, University of Connecticut, Storrs, CT 06269, USA. *These authors contributed equally to this work. Correspondence and requests for materials should be addressed to X.Y. (email: yuanx@nenu.edu.cn) or B.L. (email: baikun@engr.uconn.edu)
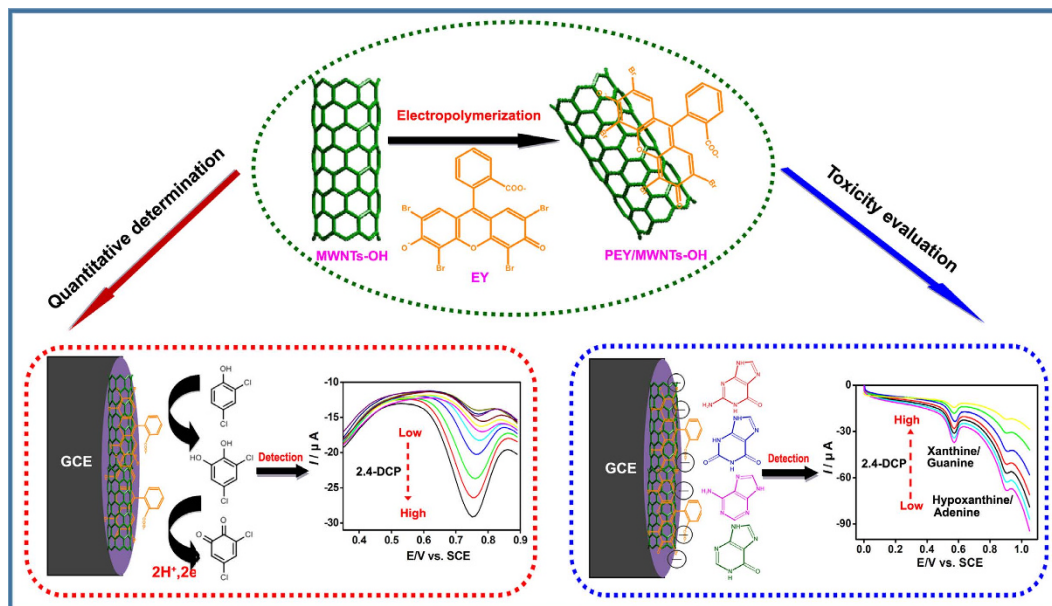
Figure 1.   Schematic illustration of PEY/MWNTs-OH/GCE and the mechanism for detecting 2,4-DCP.

study[22–24], which was based on the electrical signals of the intermediates of cellular purine metabolism, and objectively revealed the cell viability at the molecular level[25]. Graphene, carbon nanotubes, and threonine modified electrodes have been developed. Nevertheless, due to the insufficient sensitivity of these electrodes, only one electrochemical signal was detected at approximately +0.65 V corresponded to xanthine/guanine in human cancer cells. A carbon nanotubes and ionic liquid complex (MWNTs/IL) modified electrode captured two electrochemical signals ascribed to xanthine/guanine and hypoxanthine/adenine in MCF-7 cells at about +0.70 V and +1.0 V, respectively[26]. However, the electrode was fabricated by coating a MWNTs/IL paste on the electrode surface, which is difficult to control the thickness of the film. Therefore, it is critical to develop simple and stable electrodes for the sensitive determination of purine bases.

Carbon nanotubes (CNTs) have been used as the sensor material owing to their unique thermal, excellent optical and mechanical properties[27]. Although CNTs tend to entangle and hardly disperse in water because of their hydrophobic nature, they could be functionalized with different moieties to improve the solubility[28,29]. Hydroxylated multi-walled carbon nanotubes (MWNTs-OH) with π-π conjugating structure are a kind of functionalized CNTs that the structural defects can be obtained on the surface due to the sp[3] hybridization of C-C bonds formed in the functionalization process[30–32]. These defects can not only improve the solubility but also significantly enhance the reactivity and electronic property. In the same time, Eosin Y (EY), as a xanthene dye containing bromine atoms, is widely applied as the biological stain, laser dye, fluorescent probe, and sensitizer due to its high stability, versatility, and light absorptivity[33–38]. Recently, EY was successfully applied for the fabrication of electrodes to monitor catechol and hydroquinone[39], sodium dodecyl sulfate[40], and hydroquinone and catechol[41]. EY acts as the excellent electron donor, and can generate stable redox active layers by the electrochemical polymerization. However, the development of EY as sensors is still at an early stage, and it has been rarely reported to interact with carbon nanomaterials. Given the compatible structure and physical properties of MWNTs-OH and EY, hybridization might be formed via π-π interaction, through which the EY/MWNTs-OH composite would presumably produce synergic effects and exhibit higher electrocatalytic activity by improving their unique potential.

In this study, a sensitive electrode with high electrocatalytic activity toward not only 2,4-DCP but also cellular purine bases was developed, so that simple, rapid, sensitive and quantitative determination and toxicity assessment would be realized to simplify the detection and evaluation process of 2,4-DCP (Fig. 1). The poly(eosin Y)/hydroxylated multi-walled carbon nanotubes hybrid material modified glass carbon electrode (PEY/MWNTs-OH/GCE) was developed. The electrode was characterized using emission scanning electron microscopy (SEM), electrochemical impedance spectroscopy (EIS), raman spectroscopy, and cyclic voltammetry (CV) technique. The electrochemical sensor was examined for the quantitative detection and toxicity assessment of 2,4-DCP on human hepatoma (HepG2) cells for the first time that have been proved as the sensitive and stable model organisms in environmental toxicology[42].

Results and Discussion
Characterization of the PEY/MWNTs-OH/GCE.
The electrodeposition is a simple approach to immobilize organic molecules onto the electrode surface, which adjusts the surface properties including thickness, permeation, and charge transportation[43]. The successive CV curves for the electrochemical modification of PEY/GCE and PEY/MWNTs-OH/GCE were conducted over the potential range from −1.2 to +1.0 V. On the GCE (Fig. 2A), an anodic peak attributed to the oxidation of EY ($EY^{3\cdot-} - e^- \rightarrow EY^{2-}$) appeared at +0.75 V and a
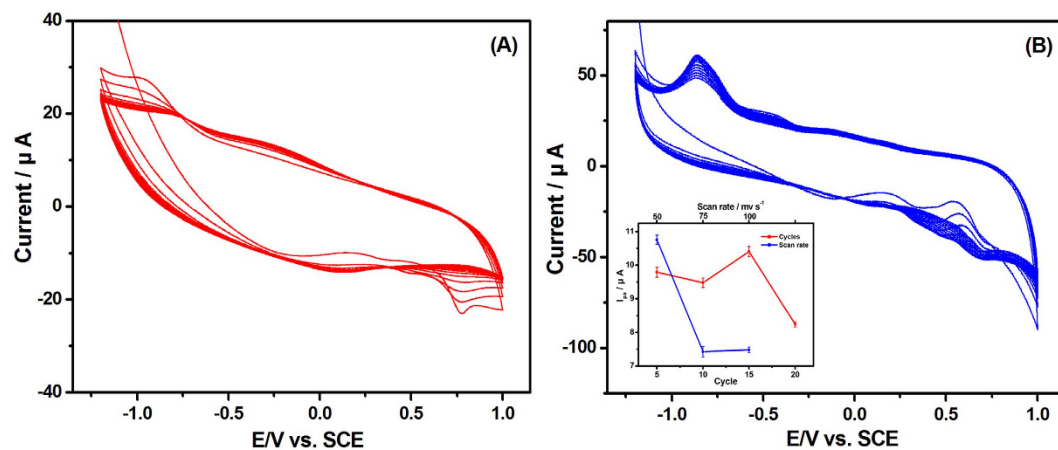
Figure 2. Electropolymerization curves of 500 μM EY in pH 5.0 PBS at (**A**) GCE and (**B**) MWNTs-OH/GCE. Inset: the influence of the cycle and scan rate on the oxidation peak current of 20 μM 2,4-DCP during the fabrication process of PEY/MWNTs-OH/GCE.
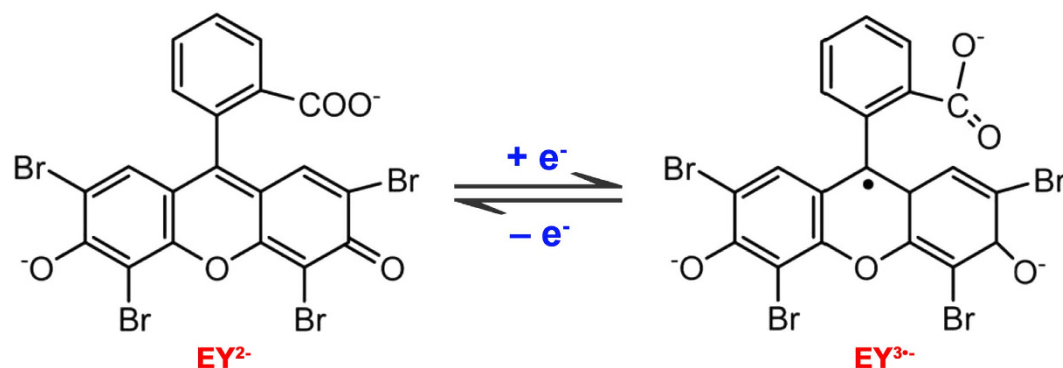

Figure 3. The structure and mechanism of electropolymerization process of EY.

cathodic peak attributed to the reduction ($EY^{2-} + e^- \rightarrow EY^{3\cdot-}$) was observed at -0.87 V in the 1st cycle. The peak current decreases with increase in number of cycles. On the MWNTs-OH/GCE (Fig. 2B), the background current was much larger than that of GCE, indicating the higher surface area of MWNTs-OH. Two oxidation and reduction peaks were found at the potential of $+0.69$ V, $+0.45$ V, -0.50 V, and -0.87 V, respectively. During the one-step electrodeposition process, the EY molecules acted as an excellent electron acceptor, which exist mainly in the form of EY^{2-} and could be reduced to EY^{3-} by the cleavage of the C=O bond on the benzene ring (Fig. 3). The obtained EY^{3-} could rapidly combine with the electrode surface[44]. The peak current was virtually constant after 15 cycles, indicating that the polymerization reached saturation at the MWNTs-OH/GCE. The thickness of the film had a significant contribution to the property of the PEY/MWNTs-OH/GCE. Thus, the influences of the cycle number and scan rate of EY on the electrocatalytic performance of PEY/MWNTs-OH/GCE were investigated (the inset of Fig. 2B). The oxidation peak current of 2,4-DCP reached to the maximum after 15 scans at the scan rate of 50 mV s^{-1}. The peak current began to drop when the polymerizing cycles were more than 15. Thick films may prevent the electron transfer process and the oxidation process. Hence, the optimal electropolymerization cycles are selected as 15 cycles.

The surface morphologies of each layer were characterized by SEM. Randomly oriented MWNTs-OH was detected with interconnected tubular structures (Fig. 4A), which was the characteristic of carbon nanotubes[45]. After the introduction of EY molecules, the EY polymer was uniformly distributed over the MWNTs-OH (Fig. 4B). The homogeneous and uniform film with three-dimensional network structure was produced, demonstrating that the EY could be modified effectively on the surface with the electrodeposition method. The highly conjugated PEY/MWNTs-OH composite exhibited high surface area, and thus providing more sites for the accumulation of the target molecule.

Then the CVs of different electrodes were studied in 5.0 mM $[Fe(CN)_6]^{3-/4-}$ containing 0.1 M KCl (Fig. 4C). The electrochemically active surface area can be obtained according to the following equation[46]:

$$i_p = (2.99 \times 10^5)nACD^{1/2}v^{1/2},$$

where i_p is the peak current, n is the number of electrons involved in the redox reaction of $Fe(CN)_6^{3-/4-}$ ($n = 1$), A is the electroactive surface area, C is the reactant concentration, D is the diffusion coefficient (6.30×10^6 cm^2 s^{-1}),
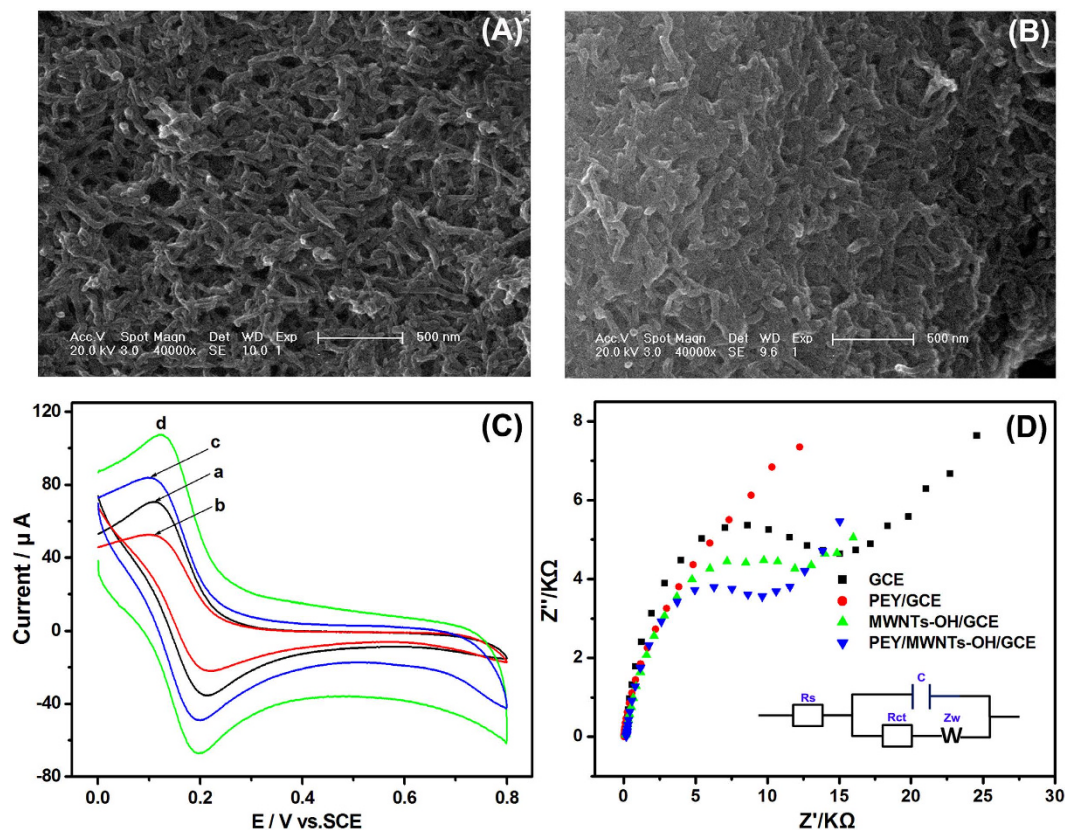
Figure 4. The SEM images of (**A**) MWNTs-OH and (**B**) PEY/MWNTs-OH; (**C**) CVs of GCE (a), PEY/GCE (b), MWNTs-OH/GCE (c), and PEY/MWNTs-OH/GCE (d) in 5.0 mM $[Fe(CN)_6]^{3-/4-}$ containing 0.1 M KCl; (**D**) EIS of different electrodes in 5.0 mM $[Fe(CN)_6]^{3-/4-}$ and 0.1 M KCl. Inset: the equivalent circuit model to fit the impedance data.

and v is the scan rate. The active surface areas for MWNTs-OH/GCE and PEY/MWNTs-OH/GCE were calculated as 0.079 cm² and 0.108 cm², respectively, which further confirmed that the PEY film increased the surface area of the MWNTs-OH/GCE.

EIS can provide details on the interfacial properties of the electrode interface during the fabrication process. The semicircular portion at higher frequencies represents the electron transfer-limited process, and the diameter corresponds to the electron transfer resistance (R_{ct})[47]. Figure 4D shows the typical Nyquist plots recorded at frequencies ranging from 0.01 to 10^5 Hz in 0.1 M KCl containing 5.0 mM $[Fe(CN)_6]^{3-/4-}$ as the electrochemical redox probe. The inset shows the equivalent circuit model to fit the impedance data. R_s, C, and W represented the solution resistance, pure capacitance, and Warburg impedance, respectively. The EIS at the bare GCE displayed a well-defined semicircle, with a huge interfacial R_{ct} of 14.3 KΩ. The increase in the R_{ct} of PEY/GCE suggested a successful modification of EY on the GCE surface. The R_{ct} decreased dramatically to 12.1 KΩ after the introduction of MWNTs-OH on the GCE, confirming an excellent electron conducting ability of MWNTs-OH. The lower R_{ct} of PEY/MWNTs-OH/GCE (9.2 KΩ) demonstrated the enhanced electron transfer reaction, which was mainly attributed to the synergistic effect between EY and MWNTs-OH.

Raman spectroscopy is a useful tool to obtain structural information of carbonaceous materials[48]. The D band corresponds to the disordered structural defects and the G band is due to the first-order scattering of the E_{2g} mode for sp² carbon lattice. The relative intensity ratio of D band to G band (I_D/I_G) can be used to examine the disorder and defects. The decrease of I_D/I_G indicated the increase in the average size of sp² domains[49]. PEY/MWNTs-OH (Fig. 5A, curve b) exhibits the D band at 1357 cm⁻¹ and the G band at 1580 cm⁻¹ with intensities lower than that of MWNTs-OH (Fig. 5A, curve a). The I_D/I_G value of MWNTs-OH was estimated to be 1.09. In the case of PEY/MWNTs-OH, the I_D/I_G value decreased to 0.78, which implied the successful formation of the PEY/MWNTs-OH hybrids and an efficient π-π interaction between them.

Voltammetric behavior of 2,4-DCP at the PEY/MWNTs-OH/GCE. The CVs of 2,4-DCP at different electrodes were investigated (Fig. 5B). No peak was observed at the GCE (curve a), which was consistent with the previous study[13]. A broad oxidation peak appeared at the PEY/GCE (curve b) but it was too weak to distinguish. In the case of MWNTs-OH/GCE, a peak at +0.78 V was observed (curve c), while a well-defined anodic peak was obtained at +0.77 on PEY/MWNTs-OH/GCE (curve d). There was no corresponding reduction peak in the inverse scan, which was the characteristic of an irreversible electrode process. The high background current of PEY/MWNTs-OH/GCE reflected its effective surface area. In addition, the peak current was 5.2 times that of
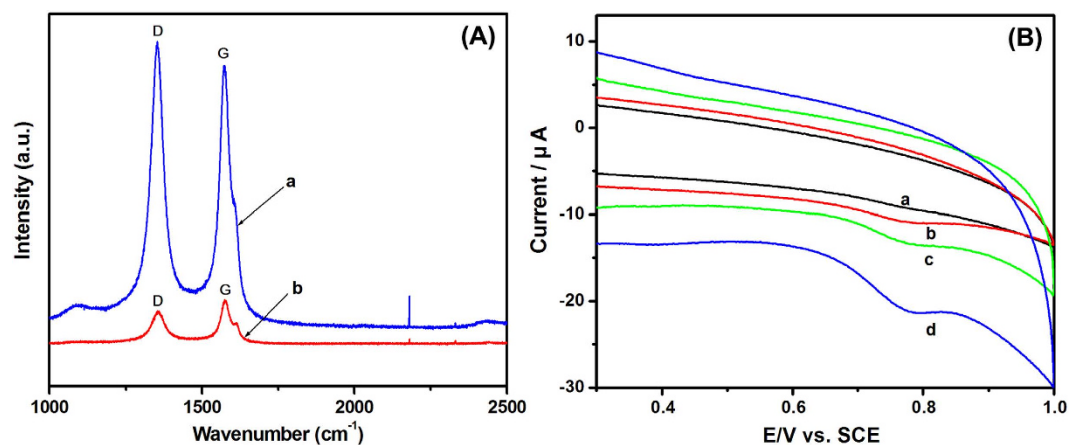
Figure 5. (**A**) Raman spectrum of MWNTs-OH (a) and PEY/MWNTs-OH nanocomposite (b); (**B**) CVs of GCE (a), PEY/GCE (b), MWNTs-OH/GCE (c), and PEY/MWNTs-OH/GCE (d) in 0.1 M pH 3.0 PBS containing 20 μM 2,4-DCP.

PEY/GCE and 2.9 times that of MWNTs-OH/GCE. Considering that graphene (Gr) was also an ideal material which can be coupled with organic dye molecules through the electron cloud overlap, the PEY/MWNTs-OH/GCE was compared with PEY/Gr/GCE (Fig. S1). The oxidation peak current of 2,4-DCP at PEY/MWNTs-OH/GCE was 2.1 times as large as PEY/Gr/GCE. The above results were caused by two reasons. First, MWNTs-OH increased the electronic conductivity, and the well-distributed poly(eosin Y) film improved the surface area for high adsorptive capability for 2,4-DCP. Second, the synergistic effect between PEY and MWNTs-OH increased the electrocatalytic activity as well as promoted the electron-transfer rate.

The experimental parameters for the detection of 2,4-DCP using the PEY/MWNTs-OH/GCE were optimized. The effects of pH on the oxidation peak current (I_p) and peak potential (E_p) of 2,4-DCP at the PEY/MWNTs-OH/GCE were studied at the pH range of 2.0–8.0 (Fig. 6A). The I_p reached to the maximum at pH 3.0 and declined obviously at pH 4.0. There was no significant change in peak current from pH 4.0 to 7.0, but the I_p decreased sharply at the pH value of 8.0, which was related to the electrochemical mechanism of 2,4-DCP. The lower pH promoted the ionization process of 2,4-DCP at the initial stages of the electrochemical oxidation, in which some phenol hydroxyl radicals were generated[50]. Meanwhile, the E_p of 2,4-DCP shifted linearly toward negative potential values with increasing the pH between 2.0 and 8.0 (inset of Fig. 6A). The linear regression equation was $E_p = -0.0662\,\mathrm{pH} + 0.975$ (R = 0.993). The slope ($-0.0662\,\mathrm{V\,pH^{-1}}$) revealed that equal numbers of electron and proton are involved in the reaction process of the 2,4-DCP[51]. Therefore, the optimum pH was selected as 3.0.

The effect of scan rate on the electrochemical characteristics of 2,4-DCP was then studied. The I_p of 2,4-DCP increased with the scan rate in the range from 30 to 200 mV s^{-1} (Fig. 6B). The linear relationship between I_p and the square root of the scan rate ($\nu^{1/2}$) can be expressed as I_p (μA) = 2.227 $\nu^{1/2}$ (mVs^{-1}) − 6.692 (R = 0.997), indicating that the electron transfer process was controlled by diffusion. Meantime, the E_p shifted positively with the increasing in the scan rate. The E_p changed linearly versus the natural logarithm of scan rate (ln ν) with a linear regression equation of E_p (V) = 0.0188 ln ν (mV s^{-1}) + 0.703 (R = 0.996). According to Laviron's theory[52], the relationship between E_p and ln ν in the irreversible electrode process could be described as

$$E_p = E^0 + \frac{RT}{\alpha nF}\,\ln\frac{RTk_s}{\alpha nF} + \frac{RT}{\alpha nF}\,\ln\,\nu$$

where ν is the scan rate, α is the electron transfer coefficient, k_s is standard rate constant, and R, T, and F have their usual meanings. α is presumed as 0.4 in the irreversible electrode process[53], and αn was easily calculated from the plot of E_p versus ln ν. The electron transfer number n is calculated to be 2. Thus, the oxidation process of 2,4-DCP on PEY/MWNTs-OH/GCE is a two-electron and two-proton process[5].

Moreover, the peak current is related to the amount of phenols accumulated on the modified electrode[54]. The influence of accumulation time and potential was investigated. The peak current of 2,4-DCP increased noticeably with raised accumulation time within 250 s (Fig. 6C). When the accumulation time was longer than 250 s, the peak current dropped slightly, indicating the 2,4-DCP reached the level of saturation. Additionally, the influence of accumulation potential was investigated (Fig. 6D), in which the maximum current was obtained at −0.30 V. Thus the optimal accumulation conditions were chosen as 250 s and −0.30 V for the electrochemical detection.

Quantitative determination of 2,4,-DCP using the PEY/MWNTs-OH/GCE.

Under the optimum conditions, the oxidation peak currents of 2,4-DCP at different concentrations on the PEY/MWNTs-OH/GCE were investigated by DPVs (Fig. 7A). The peak current of 2,4-DCP increased linearly at the concentration ranges of 5.0×10^{-9}–1.0×10^{-7} M and 2.0×10^{-7}–4.0×10^{-5} M. The linear regression equations were I_p (μA) = 14.431 c (μM) + 2.795 and I_p (μA) = 0.291 c (μM) + 5.026 with coefficients of 0.993 and 0.994, respectively (Fig. 7B). The lowest detection limit was calculated as 1.5×10^{-9} M (S/N = 3). Compared with other electrodes reported[5,10–15],
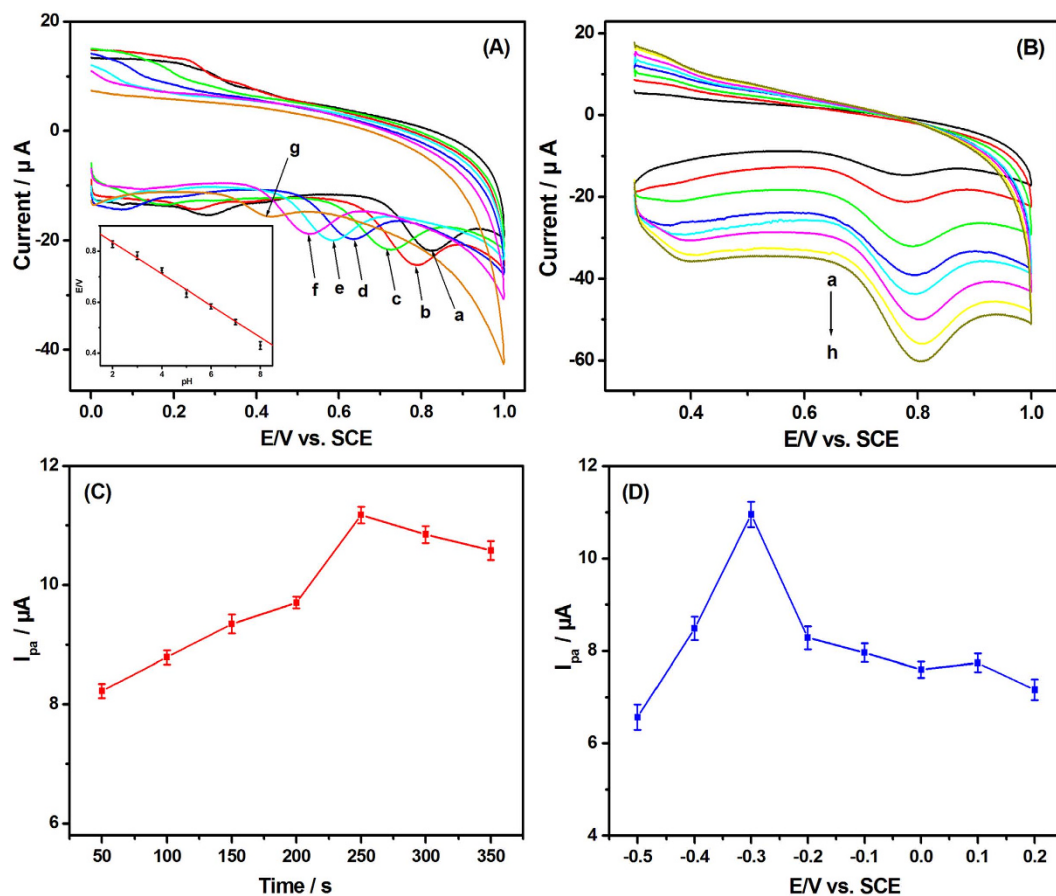
Figure 6. Influence of (**A**) pH (a–g: 2, 3, 4, 5, 6, 7, and 8), (**B**) scan rate (a–h: 30, 50, 80, 100, 120, 150, 180, and 200 mV s^{-1}), (**C**) accumulation time, and (**D**) accumulation potential on the oxidation peak current of 20 μM 2,4-DCP at the PEY/MWNT-OH/GCE. Inset: relationships between pH and the peak potential.

the PEY/MWNTs-OH/GCE electrode exhibited relatively wide linear range and low detection limit (Table 1), and thus was a promising sensor for the sensitive determination of 2,4-DCP.

The selectivity of the PEY/MWNTs-OH/GCE was investigated by adding several metal ionsand structurally similar phenols. 50-fold Mg^{2+}, Al^{3+}, Zn^{2+}, Fe^{3+}, Cu^{2+}, and Ca^{2+} had negligible effects on the electrochemical oxidation of 2,4-DCP at PEY/MWNTs-OH/GCE except for Mn^{2+} (Fig. 7C). As shown in Fig. 7D, no peak was observed for hydroquinone (a) and catechol (b) between +0.3 and +0.9 V. Although PEY/MWNTs-OH/GCE showed the electrocatalytic activity to o-nitrophenol (c), p-nitrophenol (d), 2,4,6-trichlorophenol (g) and pentachlorophenol (h), the potential differences between these phenols and 2,4-DCP were lager than 60 mV. Thus they had no influence on the peak current of 2,4-DCP (f). However, a remarkable peak was observed for 2-chlorophenol (e), and its peak potential was similar to that of 2,4-DCP. Therefore, the PEY/MWNTs-OH/GCE is applicable for the detection of 2,4-DCP in the absence of Mn^{2+} and 2-CP.

The reproducibility was investigated by six measurements of 20.0 μM 2,4-DCP with the same PEY/MWNTs-OH/GCE. The relative standard deviation (RSD) was 3.74%. Additionally, six electrodes were examined at 20.0 μM 2,4-DCP and the RSD was 4.77%. These results proved that the sensor possessed excellent reproducibility and repeatability.

Furthermore, the analytical reliability and application potential of PEY/MWNTs-OH/GCE was investigated to determine 2,4-DCP in real water samples obtained from Yitong River (Changchun, China). The recoveries ranged from 93.2% to 105.6% (Table 2) indicating the excellent reliability and applicability of PEY/MWNTs-OH/GCE.

Electrochemical behavior of HepG2 cells at the PEY/MWNTs-OH/GCE. The potential application of the PEY/MWNTs-OH/GCE in HepG2 cell suspension (3.0×10^6 cells mL^{-1}) was explored (Fig. 8A). No peak appeared on the bare GCE (curve a). A broad oxidation peak was observed at about +0.65 V at the PEY/GCE (curve b). For MWNTs-OH/GCE (curve c), an oxidation peak was obtained at +0.60 V, and an oxidation peak appeared at +0.92 V, whereas, it was too weak to recognize. With the PEY/MWNTs-OH/GCE in HepG2 cell suspension (curve d), the background current was greater than other electrodes, suggesting the more effective surface area. Meanwhile, two well-defined oxidation peaks at +0.59 V and +0.90 V attributed to xanthine/guanine, and hypoxanthine/adenine[22,23,26] were observed. The oxidation potentials shifted to less positive ones and the maximum peak currents were obtained. These results implied that the PEY/MWNTs-OH film possessed unique electrocatalytic activities toward the purine bases in HepG2 cells, and could promote electron transfer reactions.
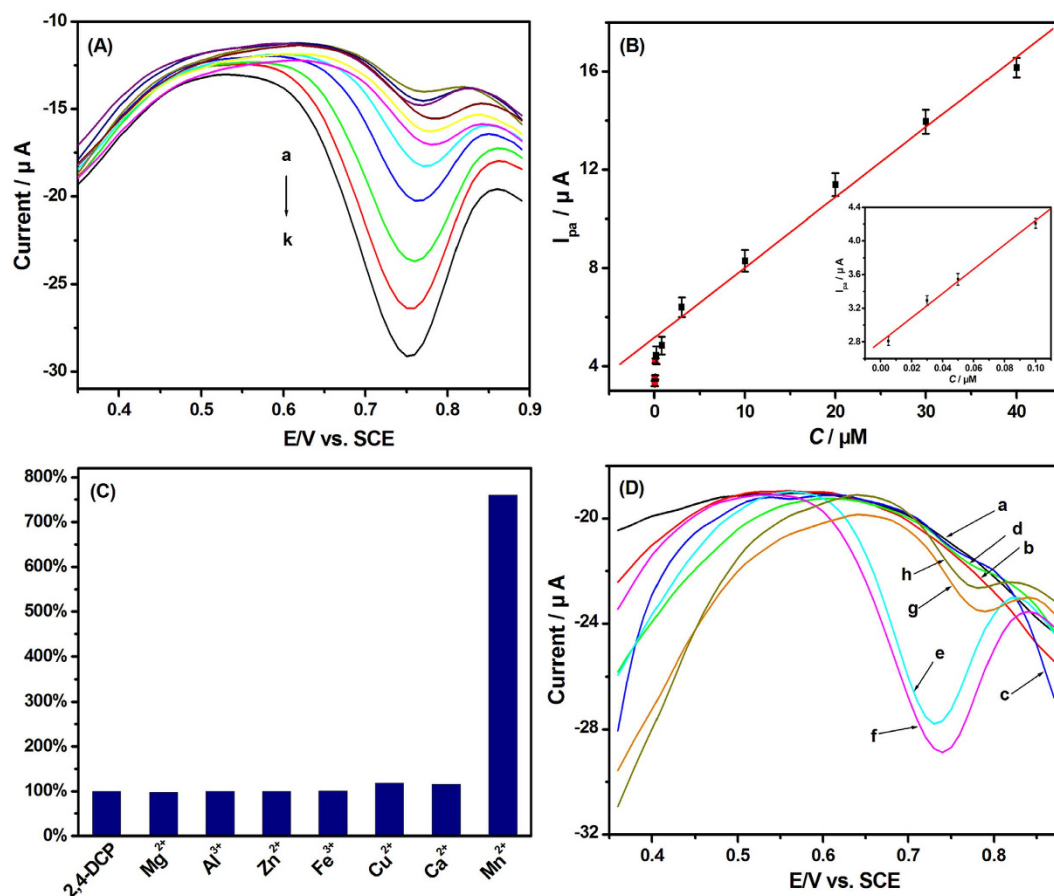
Figure 7. (**A**) DPVs of PEY/MWNTs-OH/GCE in pH 3.0 PBS with different 2,4-DCP concentrations (a–k: 0.005, 0.03, 0.05, 0.1, 0.2, 0.8, 3, 10, 20, 30, and 40 μM); (**B**) The relationship between peak current and the concentration of 2,4-DCP; (**C**) Column chart of the peak current of 20 μM 2,4-DCP containing 1 mM metal ions; (**D**) DPVs of 20 μM phenols.

Electrode	Technique	Linear range(μM)	Detection Limit (μM)	Ref.
HRP/MWNTs/GCE	Amperometry	1.0–100	0.38	10
Graphene/HRP/GCE	Amperometry	0.01–13.0	0.005	11
Nafion/MWNT/GCE	Amperometry	0.1–100	0.037	12
MB-AG/GCE	Amperometry	12.5–208	2.06	13
Nafion/PSS-GN-CTAB/GCE	LSV	0.01–2	0.002	14
MIP/GCE	DPV	5–100	1.6	15
CS/CDs-CTAB/GCE	DPV	0.04–8	0.01	5
PEY/MWNT-OH/GCE	DPV	0.005–0.1 0.2–40	0.0015	This work

Table 1. Comparison of different electrodes for detection of 2,4-DCP. HRP, horseradish peroxidase; MB-AG, myoglobin and agarose; PSS-GN-CTAB, poly(sodium-styrenesulfonate) functionalized graphene/cetyltrimethylammonium romide; MIP, molecularly imprinted polymers; CS/CDs-CTAB, chitosan/carbon dots and hexadecyltrimethyl ammonium bromide.

The influence of accumulation condition on the electrochemical signal was investigated (Fig. 8B), and 420 s was chosen as the best accumulation time.

The two electrochemical signals on PEY/MWNTs-OH/GCE were applied to describe the growth of HepG2 cells (Fig. 9). The peak currents increased gradually with the culture time within 30 h owing to the proliferation of cells. Then the peak currents reduced substantially because of the cell death caused by the lack of nutrients. These results well corresponded with the cell counting method (inset of Fig. 9), implying that the PEY/MWNTs-OH/GCE can be applied to monitor cell growth in real-time mode.

Sample	Added (μM)	Found (μM)	Recovery (%, n = 3)
Upstream water sample 1	0.1	0.099	99.0
Upstream water sample 2	1	0.932	93.2
Upstream water sample 3	5	5.28	105.6
Upstream water sample 4	20	20.4	102.0
Downstream water sample 1	0.1	0.095	95.0
Downstream water sample 2	1	0.988	98.8
Downstream water sample 3	5	4.88	97.6
Downstream water sample 4	20	20.5	102.5

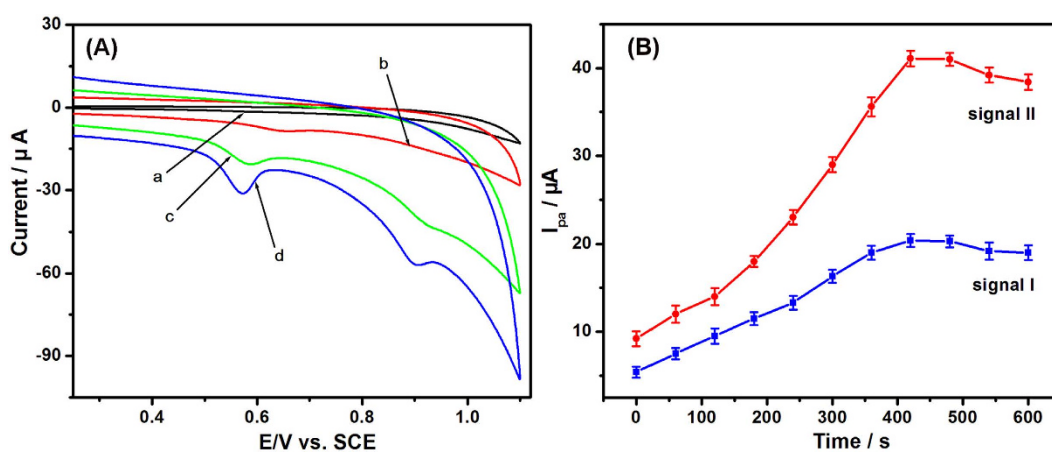**Table 2. Recovery results for 2,4-DCP in real water samples.**

Figure 8. (**A**) CVs of HepG2 cell suspension at the (a) GCE, (b) PEY/GCE, (c) PEY/MWNTs-OH/GCE, and (d) PEY/MWNTs-OH/GCE. (**B**) Influence of accumulation time on the electrochemical signals of HepG2 cell suspension. Cell inoculation concentration: 4.0×10^5 cells mL^{-1}.
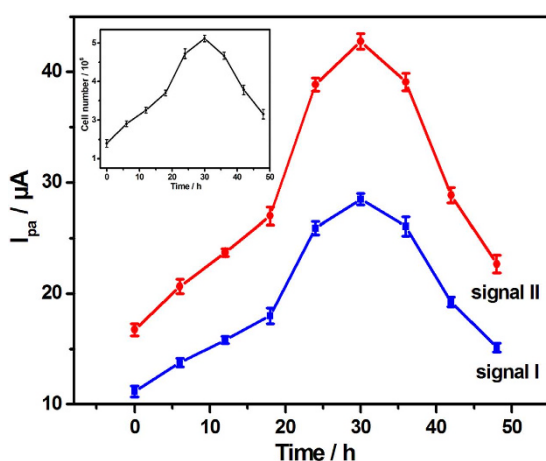

Figure 9. Growth curves of the HepG2 cells depicted by the PEY/MWNTs-OH/GCE and the cell counting method (inset).

Cytotoxicity assessment of 2,4-DCP on HepG2 cells. The electrochemical behaviors of HepG2 cells treated by 2,4-DCP at different times were investigated using PEY/MWNTs-OH/GCE (Fig. 10). Compared with
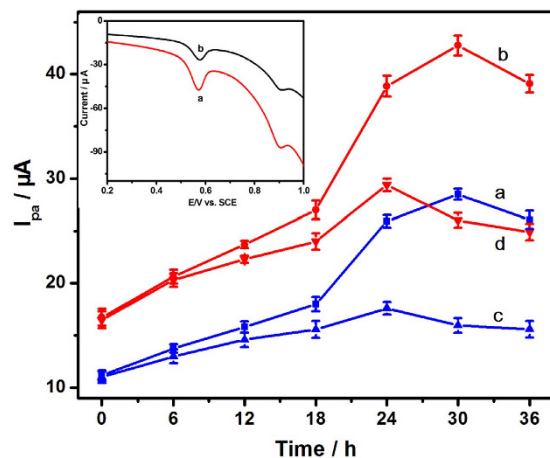
Figure 10. Dependence of the peak current of HepG2 cells on the culture time in the absence of 2,4-DCP based on electrochemical signal I (a) and signal II (b), and in the presence of 2,4-DCP based on electrochemical signal I (c) and signal II (d). Inset: CVs of HepG2 cells cultured for 30 h in the (a) absence and (b) presence of 2,4-DCP.
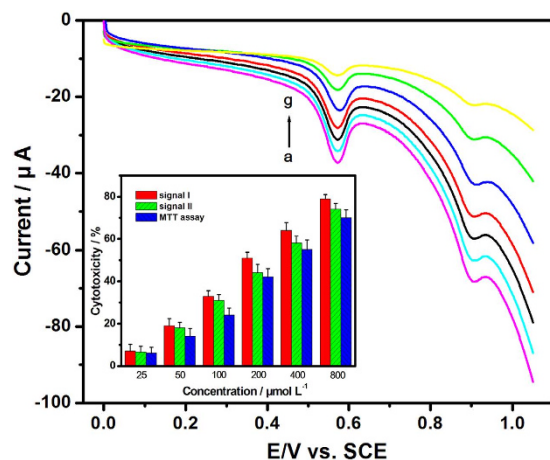

Figure 11. CVs obtained by PEY/MWNTs-OH/GCE with HepG2 cells exposed to 2,4-DCP with different concentrations (a-g: 0, 25, 50, 100, 200, 400, 800 μM). Inset: cytotoxicity of 2,4-DCP obtained by the PEY/MWNTs-OH/GCE and the MTT assay.

control groups (curves a and b), the electrochemical signal I (curve c) and signal II (curve d) of 2,4-DCP treated groups increased slowly until 24 h and then decreased ascribed to the toxicity of 2,4-DCP. Meanwhile, the peak currents of 2,4-DCP were lower than those of the control group, indicating the inhibitory effects of 2,4-DCP on HepG2 cells. A notable decrease in the electrochemical response was observed after treated by 2,4-DCP for 30 h, and the cytotoxicity reached to the maximum (inset of Fig. 10). Therefore, 30 h was chosen as the best 2,4-DCP-treated duration.

The electrochemical behaviors of HepG2 cells after treated by 2,4,-DCP with different concentrations for 30 h were studied using PEY/MWNTs-OH/GCE (Fig. 11). 2,4,-DCP exhibited significant cytotoxicity with a concentration-dependent pattern (inset of Fig. 11). The cytotoxicity (Y) was linear to the logarithm of 2,4,-DCP concentration (X) with the linear regression equations of $Y = 46.35\,X - 56.76$ (R = 0.990) for signal I and $Y = 42.50\,X - 52.12$ (R = 0.993) for signal II. The IC_{50} values based on the two electrochemical signals were 201.07 and 252.83 μM, respectively, reflecting that 2,4,-DCP had greater impacts on xanthine/guanine than those on hypoxanthine/adenine. It also confirmed the toxicity differences of 2,4-DCP to purine metabolism, which had a significance for the study of the cellular physiological process. 2,4,-DCP has been proved as a potential environmental endocrine disruptor and oxidative damage inducer[55], and can change the antioxidant enzyme activities and induce oxidative stress, a mechanism responsible for DNA damage and inhibition of cell growth[56,57]. The lower level of cell viability reduced the signals on PEY/MWNTs-OH/GCE, which related to the cellar physiological changes.

Furthermore, the conventional MTT assay was applied to compare with the result of the PEY/MWNTs-OH/GCE. The linear regression equation obtained by the MTT assay was $Y = 41.51\,X - 53.44$ (R = 0.993) and the IC_{50} value was 309.03 μM. The result verified the sensitivity of the electrochemical method on the toxicity evaluation of 2,4-DCP.

Conclusion

A novel electrochemical sensing platform was constructed in a simple and green way. The PEY/MWNTs-OH/GCE significantly facilitated the electron transfer efficiency and possessed excellent electrocatalytic activity. Under the optimal condition, it exhibited a high sensitivity, wide linear range, excellent reproducibility and good stability toward 2,4-DCP. The easy-fabricated electrode developed was also employed in real water sample analysis and showed high accuracy. Moreover, the electrochemical behavior of HepG2 cells was investigated by the PEY/MWNTs-OH/GCE. The cytotoxicity of 2,4-DCP was successfully evaluated by this electrode. This study constituted a promising tool for 2,4-DCP analysis and toxicity evaluation, and revealed a simple sensitive electrochemical approach in the field of environmental monitoring and toxicology.

Experimental Section

Materials and chemicals. The MWNTs-OH (Nanjing XFNANO Materials TECH Co., Ltd.) was 20–40 nm in diameter with purity higher than 97%. The minimum essential medium (MEM), defined fetal bovine serum (FBS) (Gibco Co., USA), penicillin, streptomycin, trypsin (Sigma, Co., USA) were used for cell culture. Dimethyl formamide and eosin Y (EY) (J&K Chemical Ltd., China) were applied for electrode fabrication. 2,4-DCP (J&K Chemical Ltd., China) was used as the target compound. Phosphate-buffered solutions (PBS) were prepared by mixing stock solutions of 0.1 M Na_2HPO_4 and 0.1 M KH_2PO_4.

Apparatus. The electrochemical measurements including cyclic voltammetry (CV) and differential pulse voltammetry (DPV) were performed on the CHI 760E electrochemical workstation (Shanghai CH Instruments, China). A three-electrode system was used, which consisted of a modified GCE as the working electrode, a saturated calomel electrode (SCE) as the reference electrode, and a platinum wire as the auxiliary electrode. The surface morphology of the nanocomposite was observed using a JEOL 6340F Scanning electron microscope (SEM). Electrochemical impedance spectroscopy (EIS) was performed using the PARSTAT 2273 potentiostat (Princeton applied research, USA). The Raman scattering spectra was obtained by the Jobin-Yvon HR 800 instrument with an Ar^+ laser source of 488 nm wavelength. The pH of the solution was measured with a PB-10 pH-meter (Sartorius Co., Germany).

Preparation of the PEY/MWNTs-OH/GCE. The glass carbon electrode (GCE) was sequentially polished using 1.0, 0.3 and 0.05 μm alumina slurry and rinsed successively with double-distilled water and ethanol solution. After 10.0 mg MWNTs-OH was dispersed with 10.0 mL dimethyl formamide using ultrasonic agitation, 5.0 μL MWNTs-OH dispersion was dropped onto GCE and dried under the infrared lamp to obtain the MWNTs-OH/GCE. Then the electropolymerization of EY was performed in PBS (pH 5.0) containing 500 μM EY and 0.3 mM KNO_3 by applying the potential (−1.2 V to +1.0 V) at 50 mV s^{-1} for 15 cycles (Fig. S2). The obtained electrode was termed as PEY/MWNTs-OH/GCE.

Cells culture and treatment. The HepG2 cells (COBIOER Biosciences Co., Ltd.) were cultured in 60 mm cell culture dish in the minimum essential medium (MEM) that was supplemented with 10% FBS, penicillin (100 μg mL^{-1}), streptomycin (100 μg mL^{-1}), 1% non-essential amino acids, and 1% sodium pyruvate at 37 °C in a humidified 5% CO_2. For the toxicity investigation, the growth medium was replaced with the medium containing 2,4-DCP. The *in-situ* cell collection was conducted as our previous study[23]. Briefly, the PBS was added to cells after the medium was removed, and then the mixture was heated in the water bath at 50 °C for 30 min to obtain the HepG2 cell suspension.

Electrochemical determination. For the electrochemical detection of 2,4-DCP, the CV was employed between +0.1 and +1.0 V with the scan rate of 50 mV s^{-1}. The DPV was performed with the following parameters: increment potential, 4 mV; pulse amplitude, 0.05 V; pulse width, 0.05 V; pulse period, 0.2 s; sample width, 50 ms. The *in vitro* toxicity of 2,4-DCP to HepG2 cells was investigated from 0.0 to +1.1 V with the scan rate of 50 mV s^{-1}. After each measurement, the PEY/MWNTs-OH/GCE was scanned for five cycles between 0.0 and +1.1 V in PBS and rinsed thoroughly with double-distilled water.

The MTT assay. HepG2 cells (1.2×10^4 cells mL^{-1}) in medium alone (200 μL) or the medium containing 2,4-DCP (200 μL) were added to the 96-well microtitre plates. 20 μL 5 mg mL^{-1} MTT was added to each well after the incubation at 37 °C for 30 h. The medium containing MTT was removed after 4 hours, and 150 μL sodium dodecyl sulfate was added. The measurement was registered on an ELX800 Microplate Reader (BioTek Instruments, Inc., USA) and determined by the absorbance values at 490 nm.

References

1. Chu, Y. Y., Wang, W. J. & Wang, M. Anodic oxidation process for the degradation of 2, 4-dichlorophenol in aqueous solution and the enhancement of biodegradability. *J. Hazard. Mater.* **180**, 247–252 (2010).
2. Xing, B. & Pignatello, J. J. Competitive sorption between 1, 3-dichlorobenzene or 2, 4-dichlorophenol and natural aromatic acids in soil organic matter. *Environ. Sci. Technol.* **32**, 614–619 (1998).
3. Zhang, X., Zha, J., Li, W., Yang, L. & Wang, Z. Effects of 2, 4-dichlorophenol on the expression of vitellogenin and estrogen receptor genes and physiology impairments in Chinese rare minnow (Gobiocypris rarus). *Environ. Toxicol.* **23**, 694–701 (2008).
4. Angelini, V. A., Orejas, J., Medina, M. I. & Agostini, E. Scale up of 2, 4-dichlorophenol removal from aqueous solutions using Brassica napus hairy roots. *J. Hazard. Mater.* **185**, 269–274 (2011).
5. Yu, L., Yue, X., Yang, R., Jing, S. & Qu, L. A sensitive and low toxicity electrochemical sensor for 2, 4-dichlorophenol based on the nanocomposite of carbon dots, hexadecyltrimethyl ammonium bromide and chitosan. *Sensor. Actuat. B-Chem.* **224**, 241–247 (2016).
6. Laurenti, E., Ghibaudi, E., Ardissone, S. & Ferrari, R. P. Oxidation of 2, 4-dichlorophenol catalyzed by horseradish peroxidase: characterization of the reaction mechanism by UV-visible spectroscopy and mass spectrometry. *J. Inorg. Biochem.* **95**, 171–176 (2003).

7. Tölgyessy, P., Vrana, B., Bartal, M., Krascsenits, Z. & Šilhárová, K. Determination of chlorophenols in sediments using ultrasonic solvent extraction followed by stir bar sorptive extraction coupled to TD-GC-MS. *Chromatographia* **69,** 389–392 (2009).

8. Chiron, S., Minero, C. & Vione, D. Occurrence of 2, 4-dichlorophenol and of 2, 4-dichloro-6-nitrophenol in the Rhône river delta (Southern France). *Environ. Sci. Technol.* **41,** 3127–3133 (2007).

9. Wang, J., Chen, G., Chatrathi, M. P. & Musameh, M. Capillary electrophoresis microchip with a carbon nanotube-modified electrochemical detector. *Anal. Chem.* **76,** 298–302 (2004).

10. Huang, S., Qu, Y., Li, R., Shen, J. & Zhu, L. Biosensor based on horseradish peroxidase modified carbon nanotubes for determination of 2, 4-dichlorophenol. *Microchim. Acta* **162,** 261–268 (2008).

11. Xu, Q. *et al.* An enzymatic amplified system for the detection of 2, 4-dichlorophenol based on graphene membrane modified electrode. *Anal. Methods* **4,** 3429–3435 (2012).

12. Arribas, A. S. *et al.* Application of carbon nanotube-modified electrodes as electrochemical sensors for the continuous monitoring of 2, 4-dichlorophenol. *Electroanalysis* **23,** 237–244 (2011).

13. Sun, Y., Wang, L. & Liu, H. Myoglobin functioning as cytochrome P450 for biosensing of 2, 4-dichlorophenol. *Anal. Methods* **4,** 3358–3363 (2012).

14. Li, J., Miao, D., Yang, R., Qu, L. & Harrington, P. D. B. Synthesis of poly (sodium 4-styrenesulfonate) functionalized graphene/cetyltrimethylammonium bromide (CTAB) nanocomposite and its application in electrochemical oxidation of 2, 4-dichlorophenol. *Electrochim. Acta* **125,** 1–8 (2014).

15. Zhang, J., Lei, J., Ju, H. & Wang, C. Electrochemical sensor based on chlorohemin modified molecularly imprinted microgel for determination of 2, 4-dichlorophenol. *Anal. Chim. Acta* **786,** 16–21 (2013).

16. Chen, J., Jiang, J., Zhang, F., Yu, H. & Zhang, J. Cytotoxic effects of environmentally relevant chlorophenols on L929 cells and their mechanisms. *Cell. Boil. Toxicol.* **20,** 183–196 (2004).

17. Nojima, T. *et al.* In-vitro derived germinal centre B cells differentially generate memory B or plasma cells *in vivo*. *Nat. Commun.* **2,** 465 (2011).

18. Fotakis, G. & Timbrell, J. A. In vitro cytotoxicity assays: comparison of LDH, neutral red, MTT and protein assay in hepatoma cell lines following exposure to cadmium chloride. *Toxicol. Lett.* **160,** 171–177 (2006).

19. Kafi, M. A., Kim, T. H., An, J. H. & Choi, J. W. Electrochemical cell-based chip for the detection of toxic effects of bisphenol-A on neuroblastoma cells. *Biosens. Bioelectron.* **26,** 3371–3375 (2011).

20. Sun, X. *et al.* Development of a novel electrochemical sensor using pheochromocytoma cells and its assessment of acrylamide cytotoxicity. *Biosens. Bioelectron.* **44,** 122–126 (2013).

21. Yoon, O. J., Kim, C. H., Sohn, I. Y. & Lee, N. E. Toxicity analysis of graphene nanoflakes by cell-based electrochemical sensing using an electrode modified with nanocomposite of graphene and Nafion. *Sensor. Actuat. B-Chem.* **188,** 454–461 (2013).

22. Zhu, X. *et al.* A novel electrochemical method to evaluate the cytotoxicity of heavy metals. *J. Hazard. Mater.* **271,** 210–219 (2014).

23. Qin, H. *et al.* An in situ electrochemical detection method of cell viability. *Analyst* **138,** 3372–3375 (2013).

24. Wu, D. M. *et al.* Voltammetric behavior of the heat-treating PC-3 cells and its application in drug sensitivity test. *Electrochem. Commun.* **13,** 623–626 (2011).

25. Guo, X. *et al.* A mini-electrochemical system integrated micropipet tip and pencil graphite electrode for detection of anticancer drug sensitivity *in vitro*. *Biosens. Bioelectron.* **64,** 594–596 (2015).

26. Li, J. *et al.* Two-signal electrochemical method for evaluation suppression and proliferation of MCF-7 cells based on intracellular purine. *Anal. Biochem.* **456,** 1–5 (2014).

27. De Volder, M. F., Tawfick, S. H., Baughman, R. H. & Hart, A. J. Carbon nanotubes: present and future commercial applications. *Science* **339,** 535–539 (2013).

28. Balasubramanian, K. & Burghard, M. Chemically functionalized carbon nanotubes. *Small* **1,** 180–192 (2005).

29. Chen, S., Shen, W., Wu, G., Chen, D. & Jiang, M. A new approach to the functionalization of single-walled carbon nanotubes with both alkyl and carboxyl groups. *Chem. Phys. Lett.* **402,** 312–317 (2005).

30. Bradley, R. H. *et al.* Surface studies of hydroxylated multi-wall carbon nanotubes. *Appl. Surf. Sci.* **258,** 4835–4843 (2012).

31. Zhao, J., Park, H., Han, J. & Lu, J. P. Electronic properties of carbon nanotubes with covalent sidewall functionalization. *J. Phys. Chem. B* **108,** 4227–4230 (2004).

32. Zhang, Y. *et al.* Photoreactivity of hydroxylated multi-walled carbon nanotubes and its effects on the photodegradation of atenolol in water. *Chemosphere* **93,** 1747–1754 (2013).

33. Nagaya, S. *et al.* Crystal structure and photoelectric conversion properties of eosin Y-adsorbing ZnO films prepared by electroless deposition. *Appl. Catal. B: Environ.* **189,** 51–55 (2016).

34. Shi, H., Cui, Y., Gong, Y. & Feng, S. Highly sensitive and selective fluorescent assay for guanine based on the Cu^{2+}/eosin Y system. *Spectrochim. Acta A* **161,** 150–154 (2016).

35. Cong, W. *et al.* Negative visualization of DNA in agarose gel by eosin Y and its related mechanism. *Analyst* **137,** 1466–1472 (2012).

36. Wang, L., Zhao, H., Chen, Y., Sun, R. & Han, B. Efficient photocatalytic hydrogen production from water over Pt–Eosin Y catalyst: A systemic study of reaction parameters. *Opt. Commun.* **370,** 122–126 (2016).

37. Hari, D. P. & König, B. Eosin Y catalyzed visible light oxidative C-C and C-P bond formation. *Org. Lett.* **13,** 3852–3855 (2011).

38. Wen, T., Li, N. B. & Luo, H. Q. A turn-on fluorescent sensor for sensitive and selective detection of sodium dodecyl sulfate based on the eosin Y/polyethyleneimine system. *Anal. Chem.* **85,** 10863–10868 (2013).

39. Ganesh, P. S. & Swamy, B. K. Voltammetric resolution of catechol and hydroquinone at eosin Y film modified carbon paste electrode. *J. Mol. Liq.* **220,** 208–215 (2016).

40. Hao, X., Lei, J. L., Li, N. B. & Luo, H. Q. An electrochemical sensor for sodium dodecyl sulfate detection based on anion exchange using eosin Y/polyethyleneimine modified electrode. *Anal. Chim. Acta* **852,** 63–68 (2014).

41. He, J. *et al.* A voltammetric sensor based on eosin Y film modified glassy carbon electrode for simultaneous determination of hydroquinone and catechol. *Anal. Methods* **6,** 6494–6503 (2014).

42. Novotnik, B., Ščančar, J., Milačič, R., Filipič, M. & Žegura, B. Cytotoxic and genotoxic potential of Cr (VI), Cr (III)-nitrate and Cr (III)-EDTA complex in human hepatoma (HepG2) cells. *Chemosphere* **154,** 124–131 (2016).

43. Chen, L., Tang, Y., Wang, K., Liu, C. & Luo, S. Direct electrodeposition of reduced graphene oxide on glassy carbon electrode and its electrochemical application. *Electrochem. Commun.* **13,** 133–137 (2011).

44. He, J. *et al.* A voltammetric sensor based on eosin Y film modified glassy carbon electrode for simultaneous determination of hydroquinone and catechol. *Anal. Methods* **6,** 6494–6503 (2014).

45. Journet, C. *et al.* Large-scale production of single-walled carbon nanotubes by the electric-arc technique. *Nature* **388,** 756–758 (1997).

46. Guo, C. X., Lei, Y. & Li, C. M. Porphyrin functionalized graphene for sensitive electrochemical detection of ultratrace explosives. *Electroanalysis* **23,** 885–893 (2011).

47. Ates, M. Review study of electrochemical impedance spectroscopy and equivalent electrical circuits of conducting polymers on carbon surfaces. *Prog. Org. Coat.* **71,** 1–10 (2011).

48. Zhu, X. *et al.* Green synthesis of a bromocresol purple/graphene composite and its application in electrochemical determination of 2, 4, 6-trichlorophenol. *Anal. Methods* **7,** 3178–3184 (2015).

49. Graf, D. *et al.* Spatially resolved Raman spectroscopy of single-and few-layer graphene. *Nano Lett.* **7,** 238–242 (2007).

50. Ureta-Zanartu, M. S. *et al.* Electrooxidation of 2, 4-dichlorophenol and other polychlorinated phenols at a glassy carbon electrode. *Electrochim. Acta* **47,** 2399–2406 (2002).

51. Li, J., Li, X., Yang, R., Qu, L. & Harrington, P. D. B. A sensitive electrochemical chlorophenols sensor based on nanocomposite of ZnSe quantum dots and cetyltrimethylammonium bromide. *Anal. Chim. Acta* **804,** 76–83 (2013).

52. Laviron, E. Adsorption, autoinhibition and autocatalysis in polarography and in linear potential sweep voltammetry. *J. Electroanal. Chem. Interfacial Electrochem.* **52,** 355–393 (1974).

53. Yin, H. *et al.* Electrochemical oxidation behavior of bisphenol A at surfactant/layered double hydroxide modified glassy carbon electrode and its determination. *J. Solid State Electr.* **15,** 167–173 (2011).

54. Zhu, X., Zhang, K., Lu, N. & Yuan, X. Simultaneous determination of 2, 4, 6-trichlorophenol and pentachlorophenol based on poly (Rhodamine B)/graphene oxide/multiwalled carbon nanotubes composite film modified electrode. *Appl. Surf. Sci.* **361,** 72–79 (2016).

55. Bukowska, B. Effects of 2, 4-D and its metabolite 2, 4-dichlorophenol on antioxidant enzymes and level of glutathione in human erythrocytes. *Comp. Biochem. Phys. C* **135,** 435–441 (2003).

56. Zhang, J., Shen, H., Wang, X., Wu, J. & Xue, Y. Effects of chronic exposure of 2, 4-dichlorophenol on the antioxidant system in liver of fresh water fish Carassius auratus. *Chemosphere* **55,** 167–174 (2004).

57. Bors, M. *et al.* Protective activity of the Uncaria tomentosa extracts on human erythrocytes in oxidative stress induced by 2,4-dichlorophenol (2,4-DCP) and catechol. *Food Chem. Toxicol.* **49,** 2202–2211 (2011).

Acknowledgements

Author Contributions

X.Y. and B.-k.L. designed and supervised the work, X.-l.Z. and K.-x.Z. fabricated the electrodes, X.-l.Z., K.-x.Z., and C.-z.W. performed the characterization, X.-l.Z. and K.-x.Z. tested the electrodes and discussed the results, X.-l.Z. wrote the manuscript, B.-k.L. and J.-n.G. revised the text, and all the authors reviewed and approved the manuscript.

Additional Information

Supplementary information accompanies this paper at http://www.nature.com/srep

Competing financial interests: The authors declare no competing financial interests.

How to cite this article: Zhu, X. *et al.* Quantitative determination and toxicity evaluation of 2,4-dichlorophenol using poly(eosin Y)/hydroxylated multi-walled carbon nanotubes modified electrode. *Sci. Rep.* **6**, 38657; doi: 10.1038/srep38657 (2016).

Publisher's note: Springer Nature remains neutral with regard to jurisdictional claims in published maps and institutional affiliations.